SN 2017ein and the Possible First Identification of a Type Ic Supernova Progenitor

Schuyler D. Van Dyk,[1] WeiKang Zheng,[2] Thomas G. Brink,[2] Alexei V. Filippenko,[3,4] Dan Milisavljevic,[5] Jennifer E. Andrews,[6] Nathan Smith,[6] Michele Cignoni,[7,8] Ori D. Fox,[9] Patrick L. Kelly,[2,10] Angela Adamo,[11] Sameen Yunus,[2] Keto Zhang,[2] and Sahana Kumar[2,12]

[1]Caltech/IPAC, Mailcode 100-22, Pasadena, CA 91125, USA 0000-0001-9038-9950
[2]Department of Astronomy, University of California, Berkeley, CA 94720-3411, USA
[3]Department of Astronomy, University of California, Berkeley, CA 94720-3411, USA 0000-0003-3460-0103
[4]Miller Senior Fellow, Miller Institute for Basic Research in Science, University of California, Berkeley, CA 94720, USA
[5]Department of Physics and Astronomy, Purdue University, 525 Northwestern Avenue, West Lafayette, IN 47907, USA
[6]Steward Observatory, University of Arizona, 933 N. Cherry Avenue, Tucson, AZ 85721, USA
[7]Dipartimento di Fisica 'Enrico Fermi', Universitá di Pisa, largo Pontecorvo 3, I-56127 Pisa, Italy 0000-0001-6291-6813
[8]INFN, Largo B. Pontecorvo 3, I-56127 Pisa, Italy
[9]Space Telescope Science Institute, 3700 San Martin Drive, Baltimore, MD 21218, USA 0000-0002-4924-444X
[10]College of Science & Engineering, Minnesota Institute for Astrophysics, University of Minnesota, 115 Union St. SE, Minneapolis, MN 55455 USA 0000-0003-3142-997X
[11]Department of Astronomy, Oskar Klein Centre, Stockholm University, AlbaNova University Centre, SE-106 91 Stockholm, Sweden 0000-0002-8192-8091
[12]Department of Physics, Florida State University, 77 Chieftain Way, Tallahassee, Florida 32306, USA

ABSTRACT

We have identified a progenitor candidate in archival *Hubble Space Telescope* (*HST*) images for the Type Ic SN 2017ein in NGC 3938, pinpointing the candidate's location via *HST* Target-of-Opportunity imaging of the SN itself. This would be the first identification of a stellar-like object as a progenitor candidate for any Type Ic supernova to date. We also present observations of SN 2017ein during the first ∼49 days since explosion. We find that SN 2017ein most resembles the well-studied Type Ic SN 2007gr. We infer that SN 2017ein experienced a total visual extinction of $A_V \approx 1.0$–1.9 mag, predominantly because of dust within the host galaxy. Although the distance is not well known, if this object is the progenitor, it was likely of high initial mass, ∼47–48 $M_\odot$ if a single star, or ∼60–80 $M_\odot$ if in a binary system. However, we also find that the progenitor candidate could be a very blue and young compact cluster, further implying a very massive (> 65 $M_\odot$) progenitor. Furthermore, the actual progenitor might not be associated with the candidate at all and could be far less massive. From the immediate stellar environment, we find possible evidence for three different populations; if the SN progenitor was a member of the youngest population, this would be consistent with an initial mass of ∼57 $M_\odot$. After it has faded, the SN should be reobserved at high spatial resolution and sensitivity, to determine whether the candidate is indeed the progenitor.

Keywords: supernovae: individual (SN 2017ein), stars: massive, binaries: general, galaxies: stellar content, galaxies: individual (NGC 3938)

1. INTRODUCTION

Supernovae (SNe) are among the most powerful explosions in the Universe and highly influential within their host galaxies throughout cosmic time. Understanding their origins, as the catastrophic endpoints of stellar evolution, is therefore an important line of inquiry in modern astrophysics. Stars more massive than ∼ 8–10 $M_\odot$ perish as core-collapse SNe (CCSNe). The most common CCSNe in the local Universe are the Type II-Plateau (SNe II-P), and we now have solid evidence that these arise from stars in the red supergiant phase (e.g., Smartt et al. 2009). The situation is less clear for SNe whose progenitor has had its H-rich envelope partially or entirely stripped away before explosion, the so-called stripped-envelope SNe (SESNe; e.g., Filippenko 1997). We now have accumulating evidence that the progenitors of Type IIb SNe (SNe IIb), stripped but still retaining ≲ 0.1 $M_\odot$ of hydrogen, appear to be yellow to somewhat blue supergiants (e.g., Maund et al. 2011; Van Dyk et al. 2011, 2014;

Folatelli et al. 2015; Bersten et al. 2018), likely in interacting binary systems of moderate mass (~ 12–$15\ M_\odot$; e.g., Podsiadlowski et al. 1993; Stancliffe & Eldridge 2009; Benvenuto et al. 2013).

For CCSNe which are hydrogen-free, there is only one identified progenitor of a SN Ib, for iPTF13bvn (Cao et al. 2013), although the actual nature of the star is still to be determined (Folatelli et al. 2016; Eldridge & Maund 2016). However, for the H-free SNe with little or no He as well, the SNe Ic, the progenitors to date have been elusive. Here we are considering normal SNe Ic; more extreme broad-lined examples of SNe Ic have been found associated with long-duration gamma-ray bursts (e.g., Hjorth & Bloom 2012). SN progenitor stars with binary companions that remain bound after explosion can evolve into many exotic configurations, including neutron star–neutron star mergers that are associated with short-duration gamma-ray bursts, kilonovae, and gravitational waves (e.g., Abbott et al. 2017).

To remove most or all of the He from the progenitor, some mechanism for extensive mass loss is required. Hachinger et al. (2012) showed that it is indeed hard to hide H and He in such SNe, so the lack of such spectral features implies the presence of efficient mass loss. One way is through a strong stellar wind from a single, massive star; for example, Georgy et al. (2009) concluded that SNe Ic would result from the explosion of a highly massive, but stripped, star in the WC or WO Wolf-Rayet (WR) phase. Dessart et al. (2012) suggested that the lack of observed He I lines in SN Ic spectra could arise from a high-mass, possibly single, progenitor. The other mass-loss mechanism is via envelope stripping in a mass-transfer binary system. Nomoto et al. (1990) modeled the SN Ic 1987M progenitor as a low-mass (~ 3–$3.5\ M_\odot$) He star, with initially 12–15 $M_\odot$, in a close interacting binary system. A low-mass binary model was also invoked to explain the SN Ic 1994I (Nomoto et al. 1994). Yoon et al. (2010) found a bimodality in their model SN Ic progenitors at solar metallicity, with lower-luminosity SNe (e.g., SN 1994I) from lower-mass ($M_{\rm ZAMS} \approx 12$–$13\ M_\odot$) binaries and a majority of SNe Ic from systems with higher-mass ($M_{\rm ZAMS} \gtrsim 33\ M_\odot$) primaries with WR wind mass loss. A similar progenitor system dichotomy had been found earlier by Wellstein & Langer (1999) and Pols & Dewi (2002). Many of the progenitors of SESNe must be lower-mass binaries, since the fraction of such SNe is locally too high to have single-star progenitors (Smith et al. 2011; see also Graur et al. 2017, e.g., their Figure 10). See also Zapartas et al. (2017) for a discussion of pathways to SESNe.

The lack of detected progenitors for SNe Ic is not for a lack of attempting to locate them. Over the last two decades, a valiant effort has been expended by a number of investigators toward detecting SN Ic progenitors. Their identification has been particularly thwarted by their proximity to luminous star clusters (e.g., SNe 2004gt and 2013dk, both in the Antennae; Gal-Yam et al. 2005; Maund et al. 2005; Elias-Rosa et al. 2013) or high extinction (Eldridge et al. 2013, who considered a number of SNe Ic), or both effects. Other influences on our ability to detect SN Ic progenitors include the available archival pre-SN imaging (e.g., Eldridge et al. 2013); moreover, massive WR stars, although bolometrically highly luminous, become optically less luminous toward the end of their lives (Yoon et al. 2012). Additionally, archival images are often not obtained in filters sensitive to the strong, broad emission lines of WR stars, particularly He II $\lambda 4686$, at which WR stars are brighter than their continua by up to 3 mag (Massey & Johnson 1998; see also Figure 7 of Shara et al. 2013).

The existing observational limits on SN Ic progenitors provide some informative constraints. Based on *HST* data, Gal-Yam et al. (2005) placed limits of $M_V > -5.5$ and $M_B > -6.5$ mag on the SN 2004gt progenitor and eliminated analogs of more than half of the known Galactic WR stars as possible progenitors. Similarly, Maund et al. (2005), from the same dataset, limited the SN 2004gt progenitor to a low-luminosity, high-temperature star, such as a single high initial mass ($> 40\ M_\odot$), carbon-rich WC star. Elias-Rosa et al. (2013) set a limit of $M_{\rm F555W} \gtrsim -5.7$ mag on the SN 2013dk progenitor luminosity and could not rule out WR stars. The observational limits in the case of either SN did not provide constraints on lower-mass binary systems. However, more recently, Johnson et al. (2017) placed astoundingly low 1σ upper limits of $M_U > -3.8$, $M_B > -3.1$, $M_V > -3.8$, and $M_R > -4.0$ mag on the presence of the SN Ic 2012fh progenitor in deep ground-based images of the host galaxy, NGC 3344, ruling out essentially all single-star models.

In this paper we describe what could be the first-ever identification and characterization of the progenitor of a SN Ic, the nearby SN 2017ein in NGC 3938. We first present early-time data on the SN itself and compare its properties to those of other well-studied SNe Ic, in particular SN 2007gr. We then show our detection of a candidate for the progenitor in archival *Hubble Space Telescope* (*HST*) images, which we isolated with high-spatial-resolution *HST* images of the SN; we initially reported this identification in Van Dyk et al. (2017). Finally, we attempt to constrain the nature of the detected
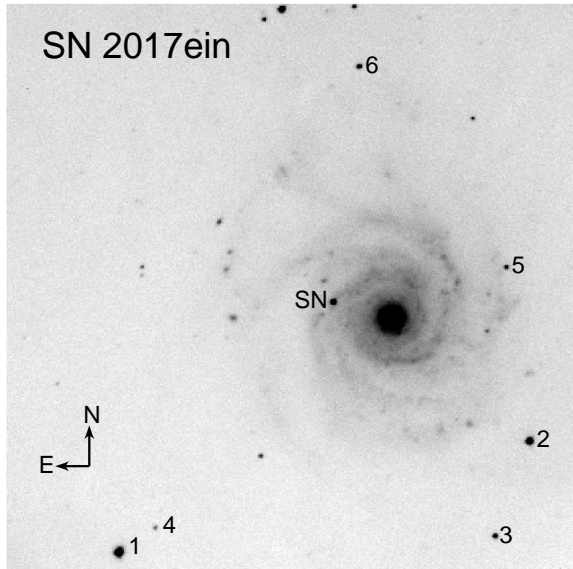
Figure 1. KAIT unfiltered image, obtained on 2017 June 26.207, of SN 2017ein and the surrounding $6'.4 \times 6'.4$ field. The SN position is indicated, along with several stars that were used as local calibrators (see Table 1) for the KAIT and Nickel SN photometry.

Table 1. Photometric Sequence for SN 2017ein[a]

Star	B	V	R	I
	(mag)	(mag)	(mag)	(mag)
1	14.383(034)	13.842(014)	13.519(016)	13.151(018)
2	15.844(034)	15.065(015)	14.613(017)	14.195(019)
3	17.721(034)	16.936(014)	16.481(016)	16.044(018)
4	18.403(035)	17.961(017)	17.691(019)	17.385(021)
5	18.207(035)	17.477(016)	17.052(018)	16.608(020)
6	18.093(033)	17.003(013)	16.380(016)	15.818(018)

[a]Uncertainties are provided in parentheses in thousandths of a magnitude.

progenitor and compare these properties to predictions from the recent models of SESN progenitors.

SN 2017ein was discovered optically by Arbour (2017) on May 25.99 (UT dates are used throughout this paper) at ~ 17.6 mag, and confirmed by *Gaia* on May 29.71 at $G \approx 16.9$ mag and given the designation Gaia17bjw[1]. The SN was classified from a spectrum obtained on May 26.6 as Type Ic, although initially as broad-lined

within one week of maximum light (Xiang et al. 2017). Im et al. (2017), through their regular monitoring of the host galaxy, were able to determine that the discovery by Arbour must have been made shortly after explosion, since the SN was detectable in their images from May 25, but not from May 24. Im et al. found that the SN was continuing to rise in brightness in early June; thus, the initial classification spectrum was most likely not obtained near maximum light. We note that NGC 3938 was also host to the SN II-L 1961U (Bertola 1963), the SN Ic 1964L (Bertola et al. 1965), and the SN II-P 2005ay (Tsvetkov et al. 2006; Gal-Yam et al. 2008).

2. OBSERVATIONS

2.1. *Ground-Based Imaging*

SN 2017ein was constantly monitored photometrically in the bands BVR_CI_C with both the 0.76-m Katzman Automatic Imaging Telescope (KAIT; Filippenko et al. 2001) and the 1-m Nickel telescope at Lick Observatory, as well as with unfiltered KAIT images, beginning within 3 days of discovery and interrupted only by nights with poor observing conditions. We followed the SN until it was no longer accessible from either KAIT or the Nickel telescope. We show a KAIT image of the field in Figure 1, with the SN indicated. From our KAIT data we measured an absolute position for the SN of 11h 52m 53.26s $+44°$ $07'26''.2$ (J2000). All images were reduced using a custom pipeline (Ganeshalingam et al. 2010). Point-spread function (PSF) photometry was then obtained using DAOPHOT (Stetson 1987) from the IDL Astronomy Users Library[2]. We also tried to perform the photometry after using the image template-subtraction method, in order to estimate the host contribution to the light. We find that the differences between using subtraction and not using subtraction are very small (< 0.1 mag) for all epochs, implying that the host contribution is minimal. We thus adopted the results without template subtraction.

Six stars in the KAIT and Nickel fields were chosen as local calibrators; they are indicated in Figure 1. This field was observed by Pan-STARRS and included in the release of the Mean Object Catalog[3]. We obtained from that release the mean PSF photometry for the six stars in the PS1 bands and used the transformations to BVR_CI_C provided by Tonry et al. (2012). We list the resulting magnitudes for the stars in Table 1 and use these for calibration of the SN photometry.

---

[1] https://wis-tns.weizmann.ac.il/object/2017ein.

[2] http://idlastro.gsfc.nasa.gov/.

[3] Available at https://archive.stsci.edu/panstarrs/.

Table 2. KAIT and Nickel Photometry of SN 2017ein[a]

MJD	B	V	R	Unfiltered	I	Source
	(mag)	(mag)	(mag)	(mag)	(mag)	
57902.27	17.18(16)	16.49(19)	16.19(20)	⋯	15.92(22)	KAIT
57903.23	16.81(18)	16.23(17)	15.95(20)	15.89(17)	15.68(19)	KAIT
57903.23	16.72(01)	16.23(06)	15.89(07)	⋯	15.63(07)	Nickel
57905.24	16.42(17)	15.81(13)	15.44(12)	15.45(12)	15.16(14)	KAIT
57906.22	16.18(16)	15.63(13)	15.33(14)	⋯	15.01(15)	KAIT
57907.26	16.03(19)	15.56(20)	15.29(20)	15.18(17)	14.91(22)	KAIT
57908.25	16.04(18)	15.39(17)	15.21(20)	15.11(20)	14.77(20)	KAIT
57909.22	15.95(17)	15.36(17)	15.05(18)	⋯	14.73(18)	KAIT
57910.20	15.84(08)	15.27(07)	14.96(12)	⋯	14.63(10)	Nickel
57910.23	16.01(20)	15.26(17)	14.98(18)	14.93(21)	14.59(19)	KAIT
57917.21	16.51(27)	15.32(21)	14.87(21)	⋯	14.52(22)	KAIT
57918.21	16.60(18)	15.36(19)	14.89(20)	15.02(23)	14.50(21)	KAIT
57919.21	16.62(18)	15.41(15)	14.92(16)	15.01(17)	14.50(18)	KAIT
57920.21	16.82(16)	15.49(16)	14.96(17)	15.06(18)	14.50(20)	KAIT
57922.21	16.98(14)	15.64(14)	15.08(16)	15.17(11)	14.57(17)	KAIT
57923.21	17.17(19)	15.68(18)	15.15(20)	15.26(18)	14.62(22)	KAIT
57924.21	17.20(16)	15.79(14)	15.21(16)	15.31(22)	14.68(16)	KAIT
57924.23	17.10(08)	15.79(12)	15.21(11)	⋯	14.70(14)	Nickel
57925.21	17.24(14)	15.90(13)	15.27(15)	15.34(11)	14.73(15)	KAIT
57925.21	17.20(09)	15.90(11)	15.28(11)	⋯	14.76(12)	Nickel
57926.23	17.40(17)	15.96(17)	15.37(18)	⋯	14.80(19)	KAIT
57927.22	17.49(17)	16.08(17)	15.46(20)	15.50(16)	14.84(19)	KAIT
57928.21	17.47(08)	16.13(09)	15.48(10)	⋯	14.90(11)	Nickel
57928.22	17.56(17)	16.16(18)	15.50(18)	15.55(18)	14.88(20)	KAIT
57929.19	17.62(24)	16.13(18)	15.56(17)	15.58(17)	14.96(19)	KAIT
57930.21	17.76(17)	16.26(15)	15.65(14)	15.67(15)	14.97(14)	KAIT
57931.23	17.78(20)	16.34(17)	15.61(19)	15.68(16)	14.99(19)	KAIT
57932.21	17.82(25)	16.41(21)	15.74(22)	15.87(31)	15.12(22)	KAIT
57933.21	17.83(16)	16.46(13)	15.81(12)	15.82(15)	15.13(13)	KAIT
57933.21	17.87(04)	16.51(02)	15.77(05)	⋯	15.12(06)	Nickel
57934.19	⋯	⋯	⋯	15.84(17)	⋯	KAIT
57938.19	18.13(27)	16.76(16)	16.08(15)	16.09(15)	15.32(15)	KAIT
57939.20	18.13(19)	16.79(14)	16.15(15)	16.13(16)	15.39(15)	KAIT
57940.19	18.32(42)	16.78(19)	16.15(19)	16.24(21)	15.42(20)	KAIT
57941.20	18.13(19)	16.91(14)	16.23(15)	16.14(16)	15.47(15)	KAIT
57942.19	18.10(35)	16.86(16)	16.21(13)	16.20(14)	15.49(16)	KAIT
57943.19	18.26(31)	16.87(17)	16.31(16)	16.26(17)	15.46(21)	KAIT
57944.19	18.43(38)	16.92(18)	16.30(19)	16.24(16)	15.58(21)	KAIT
57945.19	17.98(33)	16.83(19)	16.26(14)	16.26(18)	15.47(18)	KAIT
57947.20	18.22(23)	16.98(14)	16.30(12)	16.29(12)	15.51(15)	KAIT
57947.20	18.15(08)	17.07(09)	16.33(09)	⋯	15.55(09)	Nickel

[a]Uncertainties are provided in parentheses in hundredths of a magnitude.

Apparent magnitudes of the SN and the six calibrators were all measured in the KAIT4/Nickel2 natural system. The final results were transformed to the standard system, using the local calibrators and color terms for KAIT4 (Ganeshalingam et al. 2010; their Table 4) and updated Nickel color terms (Shivvers et al. 2017). We present the early-time KAIT and Nickel photometry of SN 2017ein in Table 2.

2.2. *Spectroscopy*

Over a two-month period beginning on 2017 June 2, eight optical spectra of SN 2017ein were obtained with the Kast Spectrograph mounted on the 3-m Shane telescope (Miller & Stone 1993) at Lick Observatory. They were taken at or near the parallactic angle (Filippenko 1982) to minimize slit losses caused by atmospheric dispersion. Data were reduced following standard techniques for CCD processing and spectrum extraction (Silverman et al. 2012) utilizing IRAF[4] routines and custom Python and IDL codes[5]. Low-order polynomial fits to comparison-lamp spectra were used to calibrate the wavelength scale, and small adjustments derived from night-sky lines in the target frames were applied. Observations of appropriate spectrophotometric standard stars were used to flux calibrate the spectra.

We obtained 3×1200 s exposures with the Blue Channel spectrograph on the MMT on 2017 June 24 (JD 2,457,928.69). The data were taken with the 1200 lines mm^{-1} grating with a central wavelength of 6360 Å and a $1\rlap{.}''0$ slit width. The seeing was $1\rlap{.}''2$. Standard reductions were carried out using IRAF, and wavelength solutions were determined using internal He-Ne-Ar lamps. Flux calibration was achieved using spectrophotometric standards at a similar airmass taken throughout the night. A log of all spectroscopic observations is provided in Table 3.

We note that we cross-checked the calibrations of our photometry and our spectra at four nearly contemporaneous epochs (MJD 57906.76, 57925.77, 57931.76, and 57935.74) by comparing observed colors with colors synthetically generated from the spectra using pysynphot[6], and found that the two datasets differed by at most ~ 0.1 mag, within the uncertainties of the photometry; thus, we are confident that our calibrations are sufficient.

2.3. *HST Imaging*

---

[4] IRAF is distributed by the National Optical Astronomy Observatory, which is operated by AURA, Inc., under a cooperative agreement with the NSF.

[5] https://github.com/ishivvers/TheKastShiv.

[6] https://github.com/spacetelescope/pysynphot.

The SN 2017ein site is in publicly available archival images obtained with the *HST* Wide Field Planetary Camera 2 (WFPC2) on 2006 October 20 (by program GO-10877, PI A. Filippenko, originally to observe SN 2005ay) in bands F555W (total exposure time 460 s) and F814W (700 s). The image mosaics were obtained from the Hubble Legacy Archive, whereas the individual WFPC2 frames were obtained from the *HST* Archive at MAST.

The SN site is just off the edge of the field of view (NIC3) of archival Near-Infrared Camera and Multi-Object Spectrograph (NICMOS) images obtained on 2003 April 3 in bands F160W, F187N, and F190N, and thus we do not consider these.

We also observed the transient itself with *HST* on 2017 June 12 using the Wide-Field Camera 3 (WFC3) UVIS channel in subarray mode, as part of our Target of Opportunity (ToO) program (GO-14645, PI S. Van Dyk), in F438W, with 10 s individual frame times and total exposure time 270 s. The F438W band was chosen in this case to attempt to avoid saturation by the SN, at which we were successful. All of these data had been initially processed via the default pipelines at STScI and were obtained from the *HST* Archive. The individual *flc* frames, which had been corrected by the pipeline for charge-transfer efficiency losses, were individually combined into an image mosaic using AstroDrizzle within PyRAF.

3. THE SUPERNOVA: EARLY RESULTS

3.1. *Photometry*

We show the combined KAIT and Nickel light curves in Figure 2. Here we have also included the photometry at R from Im et al. (2017). We compared the light curves with those of a number of SNe Ic and found that the best match was with the light curves from Hunter et al. (2009) for the normal SN Ic 2007gr in NGC 1058. The light curves for SNe 2017ein and 2007gr show quite similar behavior. We also compared the SN 2017ein light curves with those of SN 2004aw (Taubenberger et al. 2006), which may agree at early times but diverge post-peak, with SN 2004aw being generally more luminous at all bands. (We have made the comparison with SN 2004aw here, since, as we show in Section 3.5, SNe 2017ein and 2004aw could be similar bolometrically.) One can see that we missed observations of maximum light at V [$V(\mathrm{max})$] for SN 2017ein, owing to poor observing conditions. Based on the comparison with SN 2007gr, we estimate, however, that $V(\mathrm{max})$ occurred on JD $\approx 2,457,913.1$ (i.e., June 8.6).

That the SN was not detected to $R > 18.4$ mag in images obtained by Im et al. (2017) on May 24.63 (JD

Table 3. Log of Spectroscopic Observations of SN 2017ein

UT date	MJD	Age[a]	Instrument	Wavelength Range (Å)	Resolution (Å)
2017 Jun 02.26	57906.76	−6.3	Kast	3640–10,630	2.0
2017 Jun 21.27	57925.77	12.7	Kast	3626–10,710	2.0
2017 Jun 24.19	57928.69	15.6	MMT	5711–7022	0.5
2017 Jun 27.26	57931.76	18.7	Kast	3630–10,712	2.0
2017 Jul 01.24	57935.74	22.6	Kast	3636–10,710	2.0
2017 Jul 17.21	57951.71	38.6	Kast	3612–10,700	2.0
2017 Jul 26.20	57960.70	47.6	Kast	3622–10,670	2.0
2017 Jul 30.20	57964.70	51.6	Kast	3620–10,704	2.0
2017 Aug 01.19	57966.69	53.6	Kast	3620–10,680	2.0

[a]Day since estimated time of V maximum, approximately 2,457,913.1 (June 8.6).

2,457,898.13), but then was seen at $R = 17.7$ mag by these investigators on May 25.77 (JD 2,457,899.27), and later discovered by Arbour on May 25.99, would imply that the explosion date was likely sometime between JD 2,457,898 and 2,457,899. We analyzed the R-band light curve, including the Im et al. (2017) points, by fitting a simple analytic model for H-free SNe (Vacca & Leibundgut 1997; see Figure 2), and found that the explosion could have been as early as JD 2,457,898.1, or May 24.6, which we adopt. The analytic model further implies that R-band maximum (again, missed by our observations) occurred on approximately JD 2,457,916, or $\sim$ 3 days after V-band maximum.

In Figure 3 we show the early-time $B - V$, $V - R$, and $V - I$ color curves. We have initially corrected the observed color curves for Galactic foreground reddening (Schlafly & Finkbeiner 2011; via the NASA/IPAC Extragalactic Database, NED). Again, comparing with SN 2007gr (Hunter et al. 2009), we can see that the color evolution of SN 2017ein follows much the same behavior, to within the uncertainties. We also found that $V - R$ of SN 2017ein evolved at early times in a fashion similar to that of SN 2004fe (not shown; Drout et al. 2011).

3.2. *Spectroscopy*

We show the early-time spectra of SN 2017ein in Figure 4. The first spectrum was obtained on June 2, about one week after discovery (and explosion). From the light-curve comparison with SN 2007gr, we estimate the ages of the spectra relative to V(max). In the figure we also show a comparison with spectra of SN 2007gr from Valenti et al. (2008) and Chen et al. (2014), and of SN 2004aw from Taubenberger et al. (2006), at approximately the same ages. The spectra of SN 2004aw

and the Valenti et al. spectra of SN 2007gr were obtained from WISeREP[7] (Yaron & Gal-Yam 2012), and the Chen et al. SN 2007gr spectra were obtained from the UC Berkeley Supernova Database[8] One can see that the spectra of SN 2017ein resemble quite closely those of SN 2007gr, as was also true for the light curves. SN 2017ein also somewhat resembles SN 2004aw, spectroscopically, although the latter may have had somewhat broader lines. Many of the spectral features, which we have indicated in the figure, are the same between SN 2017ein and SN 2007gr, and the line widths are comparatively narrow. SN 2017ein, like SN 2007gr, is clearly not a broad-lined SN Ic.

In the pre-maximum spectrum, the features at 6350 Å and at $\sim$ 7000 Å, attributed to C II $\lambda6580$ and $\lambda7235$ in SN 2007gr (Valenti et al. 2008), are evident in SN 2017ein, and the Ca II $\lambda\lambda8542$, 8662, 8498 near-infrared (NIR) feature and, interestingly, the $\sim$ 10,400 Å feature, attributed primarily to C I, both make an early appearance. In the later spectra, Ca II, Ti II, Mg II $\lambda4481$, the well-resolved Fe II $\lambda\lambda4924$, 5018, 5169, Sc II, Na I, O I $\lambda7774$, and C I are also seen, as in SN 2007gr. For both SN 2017ein and SN 2007gr at later times, weak interstellar Hα emission appears.

We measured (see Table 4) the photospheric expansion velocity of SN 2017ein from the Fe II $\lambda\lambda4924$, 5018, 5169 and O I $\lambda7774$ absorption lines, by fitting a Gaussian to each of the lines with the routine *splot* in PyRAF. The measurements from the Fe II lines were averaged. We

---

[7] https://wiserep.weizmann.ac.il/.
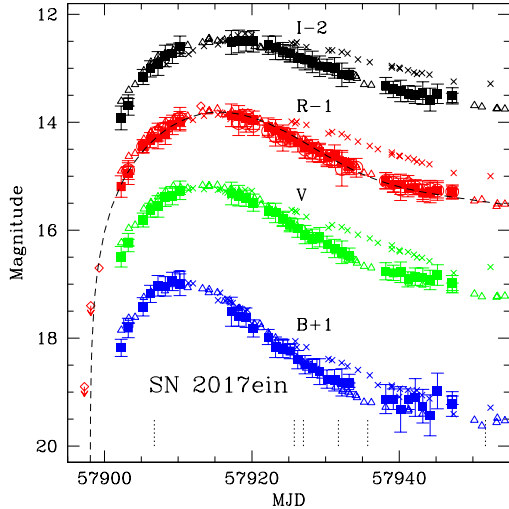[8] http://heracles.astro.berkeley.edu/sndb/. (SNDB; Silverman et al. 2012).

Figure 2. Early-time optical KAIT (solid squares) and Nickel (open squares) BVR_CI_C and KAIT unfiltered (open circles) light curves of SN 2017ein. Also shown are R observations by Im et al. (2017; open diamonds). Additionally, for comparison we show the light curves for the SNe Ic 2007gr (open triangles; Hunter et al. 2009) and 2004aw (crosses; Taubenberger et al. 2006). The curves for both SNe were shifted in time to match approximately the V maximum for SN 2017ein. After correction for reddening appropriate for these two SNe, their light curves were then reddened by the Galactic foreground for SN 2017ein and an additional host contribution of $A_V = 1.05$ mag with $R_V = 3.1$. The SN 2007gr light curves were further adjusted by a difference in distance modulus of 1.32 mag, which is consistent with the difference between the distances to the SN 2007gr and SN 2017ein hosts, to within the uncertainties; the SN 2004aw curves were adjusted by a distance modulus difference of 2.02 mag, which is a smaller difference than implied by the distance given in Taubenberger et al. The dotted lines indicate the epochs of SN 2017ein spectroscopy.

show these velocities for both sets of lines in Figure 5, with a comparison to SN 2007gr (Chen et al. 2014), SN 2004aw (Taubenberger et al. 2006), and several SNe Ic in the sample from Liu et al. (2016). The expansion velocities of SN 2017ein are not initially (soon after explosion) as high at those of SN 2007gr and SN 2004aw, and overall appear to be intermediate between these two other SNe.

Unlike SN 2007gr, though, as the Ca II NIR triplet in SN 2017ein appeared to narrow in width with advancing age, a notch of additional absorption appeared in the red wing of the triplet feature. It is unclear to what to attribute this feature; it could be the Ca II $\lambda8664$ line becoming more apparent as the triplet feature narrowed, or it could be the C I $\lambda8727$ line, which is normally
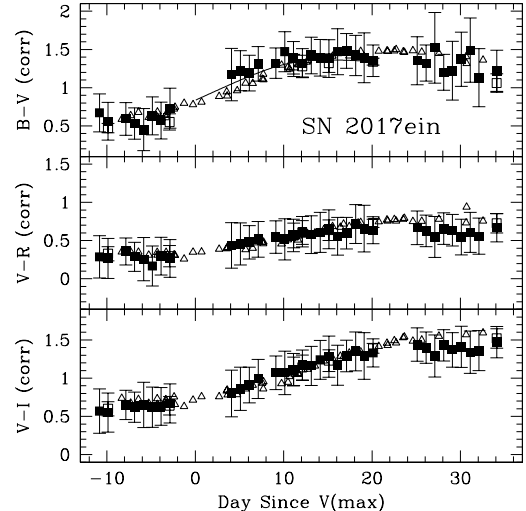

Figure 3. Early-time $B-V$, $V-R$, and $V-I$ color curves of SN 2017ein (solid squares), after initial correction for reddening attributed to the Galactic foreground contribution (Schlafly & Finkbeiner 2011). For comparison we show the color curves of SN Ic 2007gr (open triangles; Hunter et al. 2009), corrected for Galactic foreground reddening and then reddened and shifted in time to match the curves of SN 2017ein. Additionally, we show the best fit of the SN Ic color template at $B-V$ from Stritzinger et al. (2018; solid curve). See discussion in Section 3.3.

blended with the Ca II NIR triplet, as the other C I absorption features also become stronger.

Also notably exceptional for SN 2017ein is the presence of significant Na I D absorption in the June 2 spectrum (day -6.3), implying more interstellar extinction to SN 2017ein than to SN 2007gr. This is particularly seen in Figure 6, based on the MMT spectrum, in which the well-resolved Na I doublet is strong (at 5904.9 and 5910.6 Å, respectively), attributable internally to the host galaxy. The doublet is far weaker in the Galactic foreground, consistent with the assumed low reddening from this contribution. We have also indicated in Figure 6 the presumed location from the host galaxy of the diffuse interstellar band (DIB) feature at $\lambda5780$, the strength of which can be used to infer visual extinction A_V (Phillips et al. 2013) and which can change over time in a subset of SNe Ib/c (Milisavljevic et al. 2014).

3.3. *Extinction to SN 2017ein*

The extinction to SN 2017ein, as it turns out, is not well determined from our data. We first attempted to estimate the visual extinction from the SN spectra. Stritzinger et al. (2018) presented for SESNe a correlation between the equivalent width (EW) of the Na I D feature and host-galaxy A_V. From the blended
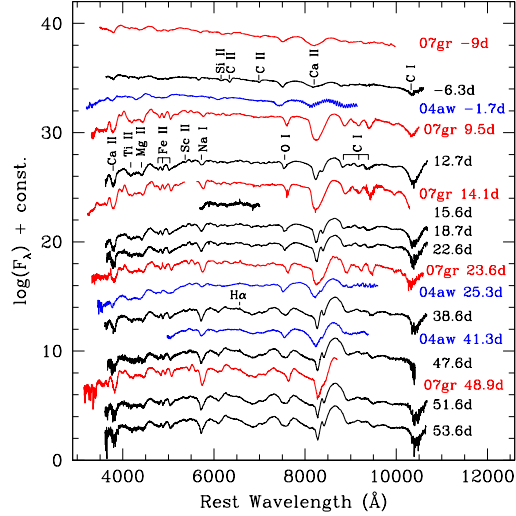
Figure 4. Early-time optical spectra obtained with the Kast spectrograph on the 3-m Shane telescope at Lick Observatory (plus one narrow-range MMT spectrum on day 15.6). The ages are relative to V maximum. For comparison we show spectra of SN 2007gr (Valenti et al. 2008; Chen et al. 2014) and SN 2004aw (Taubenberger et al. 2006) at roughly similar ages. Various absorption lines and features seen in the spectra are indicated. The SN 2017ein spectra shown in this figure are available in the electronic journal and are also posted on WISEReP, https://wiserep.weizmann.ac.il/.
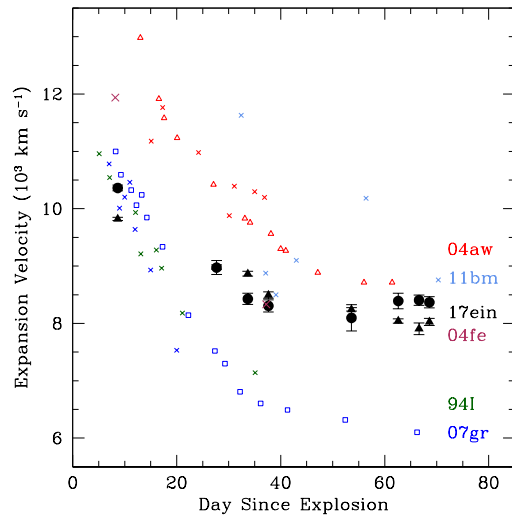
Figure 5. Expansion velocity evolution of SN 2017ein, measured from the Fe II $\lambda\lambda$4924, 5018, 5169 lines (filled squares) and O I λ7774 (filled circles). For comparison we show the velocities of SN 2007gr from the Fe II lines (Chen et al. 2014; open squares), SN 2004aw from the O I λ7774 line (Taubenberger et al. 2006; open triangles), and several SNe Ic in the sample from Liu et al. (2016; crosses) from Fe II lines.

Table 4. Photospheric Expansion Velocities for SN 2017ein

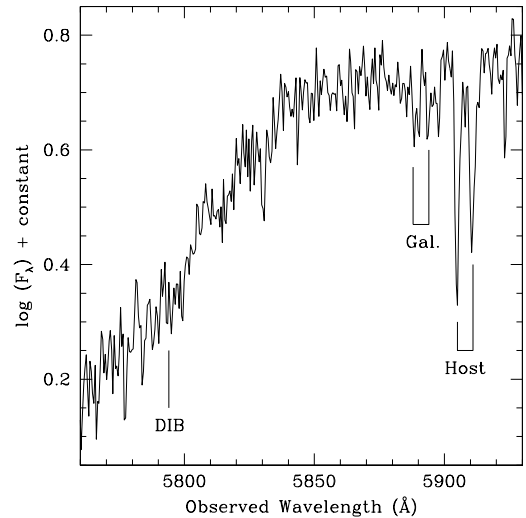| UT date	MJD	$v_{\exp}$ (Fe II)	$v_{\exp}$ (O I)
		(km s^{-1})	(km s^{-1})
2017 Jun 02.26	57906.76	9822 ± 28	10362 ± 49
2017 Jun 21.27	57925.77	8383 ± 37	8973 ± 122
2017 Jun 27.26	57931.76	8866 ± 42	8427 ± 98
2017 Jul 01.24	57935.74	8494 ± 58	8306 ± 105
2017 Jul 17.21	57951.71	8243 ± 30	8097 ± 230
2017 Jul 26.20	57960.70	8042 ± 37	8391 ± 137
2017 Jul 30.20	57964.70	7905 ± 101	8405 ± 89
2017 Aug 01.19	57966.69	8027 ± 61	8368 ± 97

Figure 6. A moderate-resolution spectrum of SN 2017ein obtained at the MMT on 2017 June 24. The interstellar Na I D doublet at the expected wavelengths for both the Milky Way ("Gal.") and NGC 3938 ("Host") are indicated. Also indicated is the expected location of the diffuse interstellar band ("DIB") near rest wavelength 5780 Å for the host galaxy.

Na I D feature in the June 2 (day −6.3) spectrum, arising entirely from the host galaxy, we measured EW= 1.61 ± 0.06 Å. From the MMT spectrum, we measured from the resolved Na I D1 and D2 lines an EW of 0.67 ± 0.04 Å and 0.72 ± 0.01 Å, respectively. The total EW of the feature from this spectrum is then 1.39 ± 0.05 Å. Referring to Stritzinger et al. (2018; their Figure 17), we then can see that A_V is somewhere in the range of 0 to ~ 2 mag. Their best fit to the relation, $A_V = 0.78(\pm 0.15) \times$ EW(Na I D), results in host $A_V = 1.26 \pm 0.29$ and $A_V = 1.08 \pm 0.25$ mag from the

Table 5. Summary of Host Extinction Estimates for SN 2017ein

Method	A_V	R_V
	(mag)	
EW(Na I D)[a]	$\sim$ 0–2	$\cdots$
	1.26 ± 0.29	$\cdots$
	1.08 ± 0.25	$\cdots$
EW(DIB λ5780)[b]	$\lesssim 1.06$	$\cdots$
$E(V - R)$[c]	1.07 ± 1.35	3.1
$E(B - V)$, $E(V - R)$, $E(V - I)$[a]	1.3–1.9	3.3–6.8
$E(B - V)$ and $E(V - R)$ only[a]	1.3–1.7	4.3
	1.0–1.2	3.1

[a] Following Stritzinger et al. (2018).

[b] Following Phillips et al. (2013).

[c] Following Drout et al. (2011).

blended feature in the Lick spectrum and the sum of the resolved lines in the MMT spectrum, respectively.

Unfortunately, the DIB λ5780 feature is not particularly distinct in the MMT spectrum. Following Phillips et al. (2013), we fit a Gaussian of 2.1 Å full width at half-maximum intensity (FWHM) to the spectrum and placed a 3σ upper limit of 203 mÅ to its equivalent width, which, from their Equation 6 (which has a 50% systematic uncertainty), corresponds to $A_V \lesssim 1.06$ mag.

We can also estimate the amount of extinction to SN 2017ein through a color-curve comparison. Drout et al. (2011), from their systematic study of SN Ib/c light curves, found that the intrinsic color, $(V - R)_0 = 0.26 \pm 0.06$ mag on $V(10\,\text{d})$, 10 days past $V(\text{max})$ (see also Bianco et al. 2014 and Dessart et al. 2016). For SN 2017ein, we estimate that $V(10\,\text{d})$ was about JD 2,457,923.1, and on that day, $V - R = 0.49 \pm 0.27$ mag. The Galactic foreground contribution to $E(V - R)$ is quite small, 0.012 mag (Schlafly & Finkbeiner 2011). This would indicate that the host contribution to $E(V - R)$ is 0.22 ± 0.28 mag for SN 2017ein, where the uncertainty includes both the measurement uncertainty in the SN 2017ein $V - R$ color from KAIT and the uncertainty in the Drout et al. (2011) intrinsic color. Assuming a Fitzpatrick (1999) reddening law and $R_V = 3.1$, this corresponds to $A_V = 1.07 \pm 1.35$ mag.

We compared the SN 2017ein $B - V$ curve, corrected for the low Galactic foreground reddening (0.019 mag), with that of SN 2007gr, for which the Galactic reddening is $E(B - V) = 0.055$ mag (Chen et al. 2014; via Schlafly & Finkbeiner 2011) and the host reddening is assumed to be quite low (Hunter et al. 2009; Drout et al. 2011; Chen et al. 2014); see Figure 3. Additionally, Stritzinger et al. (2018), based on their sample from the Carnegie SN Project (CSP), provided color templates, after correction for Galactic foreground reddening, for SESNe, specifically for SNe Ic, from 0 d to +20 d relative to $V(\text{max})$. The relevant template to apply here is for $B - V$, which we show compared to the color curve for SN 2017ein in Figure 3. (Two other templates from Stritzinger et al. 2018, $V - r$, and $V - i$, might have been applicable here; however, it is not readily evident how to transform accurately for SNe Ic between the SDSS r and i bands used by the CSP and the Johnson-Cousins R_C and I_C bands which we used for this study.) Both the template and the SN 2007gr $B - V$ color curve imply that $E(B - V) = 0.34 \pm 0.07$ mag for SN 2017ein. From a minimum χ^2 fitting of the SN 2017ein color curves to the corresponding SN 2007gr ones, we estimate that $E(V - R) = 0.24 \pm 0.06$ and $E(V - I) = 0.57 \pm 0.06$ mag for SN 2017ein (the Galactic foreground contribution to $E(V - I)$ is 0.026 mag). The value of $E(V - R)$ for the entire color curve is consistent with that inferred from the Drout et al. (2011) fiducial value at $V(10\,\text{d})$.

We performed an analysis of the three color excesses in a manner similar to that of Stritzinger et al. (2018), assuming a Fitzpatrick (1999) reddening law. We fit the values of host A_V and R_V that were best constrained by all three excesses. We found a rather large range in both parameters, $A_V = 1.3$–1.9 mag for $R_V = 3.3$–6.8. Immediately, these imply that the visual extinction to SN 2017ein is appreciable, consistent with the large range in A_V inferred from the Na I D feature strength, and that the dust is dissimilar from the diffuse Galactic component (for which $R_V = 3.1$). Stritzinger et al. (2018) have indeed argued that $R_V = 4.3$ is typical for SNe Ic, consistent with their general location in dusty environments presumably comprised of larger dust grains (we note, however, that this inference is based on only one of the events in their sample, which had more extreme reddening). Values of R_V larger than 3.1 are typical for massive star-forming regions; for example, Smith (2002) found that the local $R_V = 4.8$ for clouds in the Carina Nebula. This effect likely arises from the strong ultraviolet radiation from young O-type stars which destroys some of the smallest grains, leading to a flatter reddening law.

The high values of A_V and R_V are most strongly driven in our analysis by the value of $E(V - I)$. If we relax our analysis and consider only $E(B - V)$ and $E(V - R)$, and if we further assume that $R_V = 4.3$ (see

above), then A_V would be in the range of 1.3–1.7 mag, consistent with the range in A_V when including all three color excesses. If we, however, assume that $R_V = 3.1$, similar to Galactic diffuse interstellar dust, then A_V would be distinctly lower, 1.0–1.2 mag. For the sake of discussion below, specifically when we analyze the nature of the SN progenitor in Section 4.3, we will consider all three ranges in extinction and their implications.

We summarize all of the host-galaxy extinction estimates for SN 2017ein in Table 5. If a value for R_V is either estimated or assumed, it is indicated in the table as well.

3.4. Distance to SN 2017ein

Another quantity for SN 2017ein that is not well known is its distance, D. Several estimates exist for the distance to the host galaxy, NGC 3938. Poznanski et al. (2009), based on assuming that SNe II-P are standardizable candles, estimated that the distance modulus to SN 2005ay is $\mu = 31.27 \pm 0.13$ mag ($D = 17.9$ Mpc). Rodríguez et al. (2014), invoking a similar, color-based standardization of the absolute brightness of SNe II-P, found that $\mu = 31.75 \pm 0.24$ mag (22.4 Mpc) for their method in the V band and 31.70 ± 0.23 mag (21.9 Mpc) in I. Several early Tully-Fisher estimates (Bottinelli et al. 1984; 1986) resulted in far shorter distances, with $\mu \approx 28.7 \pm 0.7$ mag ($D \approx 5.7$ Mpc), although Tully (1988) lists $\mu = 31.15 \pm 0.40$ mag (17.0 Mpc)[9].

We therefore consider hereafter a range in possible distance moduli to SN 2017ein of 31.15 to 31.75 mag ($D = 17.0$ to 22.4 Mpc). Given this distance range and the inferred SN extinction, above, for SN 2017ein, $M_V(\mathrm{max}) \approx -16.9$ to -17.5 mag, which is consistent with -17.2 mag for SN 2007gr (Hunter et al. 2009), but less luminous than -18.0 mag for SN 2004aw (Taubenberger et al. 2006).

3.5. Quasi-Bolometric Light Curve

We constructed an early-time bolometric light curve of SN 2017ein from our observed BVR_CI_C light curves. Given the relative sparseness in the photometric coverage and the large ranges in both distance and reddening, high precision was not a particular concern. For that reason, rather than performing our own detailed blackbody fitting of each set of photometric points, we utilized the relations for SESNe from Lyman et al. (2014) for estimating bolometric corrections to the absolute B and V light curves based on the reddening-corrected colors, in order to generate the SN 2017ein bolometric light
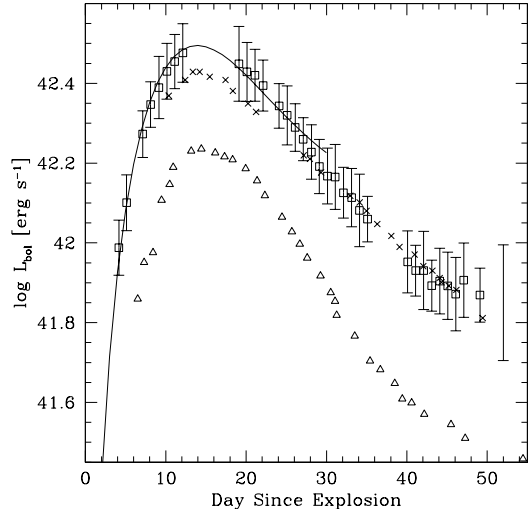
---

9 See also the Extragalactic Distance Database, http://edd.ifa.hawaii.edu/.

Figure 7. Quasi-bolometric light curve of SN 2017ein (open squares), assuming the bolometric corrections for SESNe from Lyman et al. (2014). The uncertainties shown with each data point arise primarily from the photometric measurements and from the uncertainties in the bolometric corrections. An error bar is also given, representing the additional uncertainty in both the reddening and the distance. For comparison we show the bolometric light curves for SN 2007gr (Hunter et al. 2009; Chen et al. 2014; open triangles) and SN 2004aw (Taubenberger et al. 2006; crosses). Additionally, we display the mean best-fit Arnett (1982) semi-analytical model (solid curve), powered by radioactive decay of ^{56}Ni and ^{56}Co.

curve. We show this curve in Figure 7. Although there are uncertainties in both the photometry and the bolometric corrections, these are dwarfed by the overall uncertainties in both the distance and the extinction to the SN.

For comparison we also show in Figure 7 the bolometric light curves of SN 2007gr (Hunter et al. 2009; Chen et al. 2014) and SN 2004aw (Taubenberger et al. 2006). The bolometric luminosity of SN 2017ein is consistent at peak, to within the large uncertainties, with that of SN 2007gr; however, overall, the former is generally more luminous than the latter. SN 2004aw, which was more luminous than SN 2007gr, is in agreement with SN 2017ein, to within the uncertainties.

We have modeled the bolometric luminosity via a semi-analytical light curve, following the method of Arnett (1982; see also Valenti et al. 2008; Cano 2013; Taddia et al. 2015; Lyman et al. 2016; Prentice et al. 2016; Arnett et al. 2017). The best-fit model to the bolometric luminosity implies that the maximum bolometric luminosity, $L_{\mathrm{bol}}(\mathrm{max})$, is (1.7–3.4) $\times 10^{42}$ erg s^{-1}, and the maximum occurred around day 14 since explo-

Table 6. Comparison of Light-Curve-Derived Parameters for SN 2017ein

SN	$M(^{56}\mathrm{Ni})$	M_{ej}	E_{K}	Source
	$(M_\odot)$	$(M_\odot)$	$(10^{51}\ \mathrm{erg})$	
2017ein	0.10–0.17	0.96–1.76	0.54–0.99	This work[a]
$\cdots$	0.05–0.2	$1.2^{+0.3}_{-0.2}$	$0.7^{+0.2}_{-0.1}$	This work[b]
2007gr	0.061 ± 0.014	$\cdots$	$\cdots$	Chen et al. (2014)[a]
$\cdots$	0.076 ± 0.020	2.0–3.5	1–4	Valenti et al. (2008); Hunter et al. (2009)[a]
$\cdots$	$\cdots$	~ 1.0	$\cdots$	Mazzali et al. (2010)[c]
$\cdots$	$0.07^{+0.01}_{-0.01}$	$1.2^{+0.6}_{-0.4}$	$0.8^{+0.3}_{-0.3}$	Drout et al. (2011)[b]
2004aw	0.25–0.35	3.5–8.0	3.5–9.0	Taubenberger et al. (2006)[a]; Mazzali et al. (2017)[c]
$\cdots$	$0.27^{+0.05}_{-0.05}$	$4.5^{+2.1}_{-1.3}$	$2.8^{+1.3}_{-0.8}$	Drout et al. (2011)[b]
SN Ic sample	0.33 ± 0.07	5.75 ± 2.09	1.75 ± 0.24	Taddia et al. (2015)[a]
$\cdots$	0.24 ± 0.15	$1.7^{+1.4}_{-0.9}$	$1.0^{+0.9}_{-0.5}$	Drout et al. (2011)[b]

[a] From the quasi-bolometric light curve.

[b] From multiband light curves.

[c] From analysis of nebular spectra.

sion. We show the mean of the best-fit model in Figure 7.

The Arnett (1982) model (see, e.g., Equations A1 and A2 of Valenti et al. 2008; Equations 1 and 2 of Cano 2013) fits two parameters, the nickel mass $M(^{56}\mathrm{Ni})$ and the diffusion timescale τ_{m}, where $\tau_{\mathrm{m}}^2 = (C\kappa_{\mathrm{opt}}M_{\mathrm{ej}})/(\beta c v_{\mathrm{sc}})$. In this expression, M_{ej} is the SN ejecta mass, c is the speed of light, β is a constant of integration ~ 13.8 (Arnett 1982), v_{sc} is the scale velocity, κ_{opt} is the optical opacity (often assumed to be $0.07\,\mathrm{cm}^2\,\mathrm{g}^{-1}$), and C is a constant of proportionality. Note that the M_{ej} estimate is just for the mass involved in the diffusion of SN light; if nonionized ejecta mass also exists, the value of M_{ej} could be larger (Wheeler et al. 2015). The quantity v_{sc} is generally assumed to be the photospheric velocity (v_{ph}) at maximum light. Note that, for example, Lyman et al. (2016) assumed that $C = 2$, whereas Chatzopoulos et al. (2012) assumed $C = 10/3$ (since, generally, the mean photospheric velocity is adopted, rather than the peak velocity, at optical depth 1/3). The kinetic energy of the ejecta is $E_K = (3/10)M_{\mathrm{ej}}v_{\mathrm{sc}}^2$. From our fitting, the value of $\tau_{\mathrm{m}} = 11.6\,\mathrm{d}$. Based on our measurement of velocities from the Fe II lines (assumed to be nearly photospheric) in the observed spectra, we have set $v_{\mathrm{ph}} = 9700\,\mathrm{km\,s}^{-1}$.

The results of the modeling are that $M(^{56}\mathrm{Ni})$ is in the approximate range 0.09–0.18 $M_\odot$. If $\kappa_{\mathrm{opt}} = 0.07\,\mathrm{cm}^2\,\mathrm{g}^{-1}$, then for SN 2017ein, $M_{\mathrm{ej}} \approx 1.45\,M_\odot$ and, thus, $E_K \approx 8.1 \times 10^{50}\,\mathrm{erg}$. For comparison with SN 2007gr, $M(^{56}\mathrm{Ni}) \approx 0.06\,M_\odot$ (Chen et al. 2014) to

$\sim 0.08\ M_\odot$ (Valenti et al. 2008; Hunter et al. 2009), and Hunter et al. (2009) estimated that $M_{\mathrm{ej}} \approx 2.0$–3.5 $M_\odot$ and $E_K \approx (1\text{–}4) \times 10^{51}\,\mathrm{erg}$. From nebular spectra of SN 2007gr, Mazzali et al. (2010) estimated a lower $M_{\mathrm{ej}} \approx 1\,M_\odot$. In contrast, Taubenberger et al. (2006) found for SN 2004aw significantly higher values of $M(^{56}\mathrm{Ni}) = 0.25$–0.35 $M_\odot$, $M_{\mathrm{ej}} = 3.5$–8.0 $M_\odot$, and $E_K = (3.5\text{–}9.0) \times 10^{51}\,\mathrm{erg}$ (see also Mazzali et al. 2017). We note that Taddia et al. (2015), from their sample of SNe Ic, estimated mean values of $M(^{56}\mathrm{Ni}) = 0.33\,M_\odot$, $E_K = 1.75 \times 10^{51}\,\mathrm{erg}$, and large $M_{\mathrm{ej}} = 5.75\,M_\odot$. We summarize this comparison in Table 6.

We can also analyze these parameters, $M(^{56}\mathrm{Ni})$, M_{ej}, and E_K, from the observed light curve, following Drout et al. (2011). From the simple analytic model we constructed for the R-band light curve (see Section 3.1), we found that $M_R(\mathrm{max}) \approx -17.1$ to $-18.6\,\mathrm{mag}$ for SN 2017ein, given the distance and extinction range. From this model, the quantity Δm_{15}, the decrease in brightness between maximum and 15 days post-maximum, is 0.87 mag. This Δm_{15} value is consistent with that of SN 2007gr, to within the uncertainties (Drout et al. 2011). From $M_R(\mathrm{max})$ and Δm_{15}, we found that $M(^{56}\mathrm{Ni}) \approx 0.05$–0.2 $M_\odot$, which agrees well with that found from the bolometric curve. From the simple model, the characteristic width of the light curve is $\tau_c = 10 \pm 1\,\mathrm{d}$ (again, consistent with SN 2007gr; Drout et al. 2011). For $v_{\mathrm{ph}} = 9700\,\mathrm{km\,s}^{-1}$, we can then infer that $M_{\mathrm{ej}} \approx 1.2\,M_\odot$ and $E_K \approx 7 \times 10^{50}\,\mathrm{erg}$ for SN 2017ein. Again, these

are completely consistent both with what we found (above) for the bolometric light-curve analysis and with SN 2007gr. We note that Drout et al. (2011) found much higher values for these various parameters for SN 2004aw: $\tau_c \approx 19$, $M(^{56}\text{Ni}) \approx 0.27\,M_\odot$, $M_{\text{ej}} \approx 4.5\,M_\odot$, and $E_K \approx 2.8 \times 10^{51}$ erg.

4. THE SUPERNOVA PROGENITOR

4.1. *Progenitor Identification*

To possibly identify a progenitor candidate in the 2006 *HST* images, we astrometrically registered the 2006 WFPC2 F555W image mosaic to the 2017 WFC3 image mosaic. Using 27 fiducial stars, we were able to register the images to 0.26 WFPC2/WF pixel [1σ root-mean square (rms); 26 milliarcsec]. As a result, SN 2017ein would be at (798.55, 1766.58) in the WFPC2 image mosaic. An object can be seen at (798.33, 1766.54). This is a difference of 0.22 pixel, which is within the rms uncertainty in the astrometry. We therefore consider this object to be a candidate for the progenitor of SN 2017ein. Note that we first preliminarily identified this object in Van Dyk et al. (2017). We show the WFC3 and WFPC2 images to the same scale and orientation in Figure 8.

We have analyzed this object further by performing PSF-fitting photometry of the *HST* WFPC2 images using Dolphot (Dolphin 2000; 2016). Prior to this step, we processed the individual WFPC2 frames with AstroDrizzle, to attempt to flag cosmic-ray hits. We set the Dolphot parameters FitSky=3 and RAper=8, using the TinyTim PSFs provided with Dolphot and setting the parameters InterpPSFlib and WFPC2useCTE to "true." The SN site is contained in the WFPC2 chip 2. We find 24.56 ± 0.11 and 24.58 ± 0.17 VEGAMAG in F555W and F814W, respectively. Dolphot also outputs "object type"="1" for the source, which indicates that the routine considers it to be a "good star." Other indicators also point to a star-like character: the sharpness and crowding parameters in each band are 0.002 and -0.007, and 0.030 and 0.076, respectively. The signal-to-noise ratio (SNR) in each band for the star is appreciable, ~ 10 and ~ 6 in F555W and F814W, respectively. The output photometric quality flag from Dolphot is also "0" for both bands, meaning (from the Dolphot documentation) that the star was recovered very well in the image data. The observed color of the source is F555W$-$F814W$= -0.02 \pm 0.20$ mag.

4.2. *Metallicity of the Supernova Site*

We can estimate the metallicity at the SN 2017ein site from the oxygen abundance gradient for NGC 3938 presented by Pilyugin et al. (2014). Oxygen abundance is
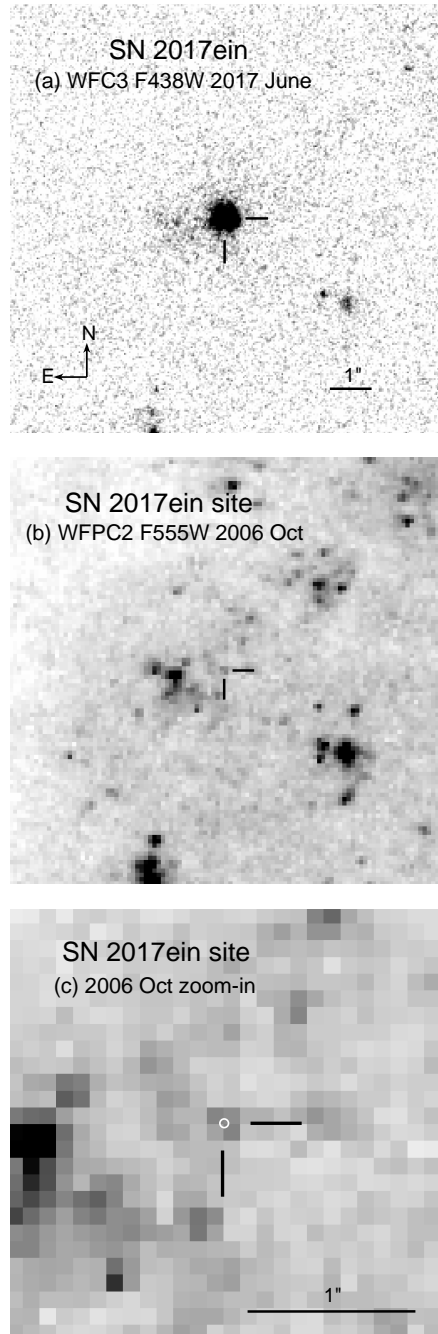
Figure 8. (a) A portion of the WFC3/UVIS image of SN 2017ein obtained in F438W on 2017 June 12. The position of the SN is indicated with tickmarks. (b) A portion of the WFPC2 image of the host galaxy, NGC 3938, in F555W on 2006 October 20, at the same orientation and scale as panel (a). (c) A zoom-in of panel (b), with the SN position indicated by a white circle with radius equal to the 0.26 pixel rms astrometric uncertainty. The location of the SN is also indicated in all three panels with tickmarks. We consider the identified object to be the candidate progenitor of SN 2017ein. North is up, east is to the left in the figure.

often used as a proxy for metallicity. In that study the central oxygen abundance is $12+\log(\mathrm{O/H}) = 8.79\pm0.05$ and the gradient is $-0.0413\pm0.0066\,\mathrm{dex\,kpc^{-1}}$. We deprojected an image of the host galaxy from the Digitized Sky Survey, assuming the position angle ($29°$) and inclination ($18°$) from Jarrett et al. (2003), and calculate that the SN is $44''$ from the host nucleus. Given the range in host-galaxy distance (above), this corresponds to a ~ 3.7–$4.8\,\mathrm{kpc}$ nuclear offset, and with this range we estimate, from the published abundance gradient, that $12 + \log(\mathrm{O/H}) \approx 8.59$–$8.64$.

Nebular Hα and [N II]$\lambda6583$ emission are also seen in the MMT spectrum from June 24. Although not an ideal strong-line indicator, the ratio of the line fluxes, [N II]$\lambda6583$/Hα, known as the N_2 index (Pettini & Pagel 2004), provides an estimate of metallicity. Dereddening the spectrum assuming both $A_V = 1\,\mathrm{mag}$ (with $R_V = 3.1$), we obtain $N_2 = -0.30$. If the extinction in the SN environment were as high as $A_V = 2\,\mathrm{mag}$, the index varies slightly, to -0.31. Following the calibration of this index by Marino et al. (2013), this would imply that $12 + \log(\mathrm{O/H}) \approx 8.60$.

If we adopt the oxygen abundance for the Sun as $12+\log(\mathrm{O/H}) \approx 8.69$ (Asplund et al. 2009), we can infer that the metallicity at the SN site is somewhat subsolar (i.e., $[\mathrm{Fe/H}] \approx -0.10$).

4.3. *The Nature of the Progenitor Candidate*

Assuming that the extinction to the SN we have estimated applies to the progenitor candidate as well, and given the assumed range in distance, we find that the object is consistent with being quite luminous and blue. (Note that we are only considering here interstellar extinction, which provides a lower limit on the total extinction in the presence of any circumstellar extinction destroyed by the SN breakout; although not typically expected for hot blue stars, some binary WC stars are surrounded by dust formed by colliding winds; e.g., Williams 2008.) We show in Figure 9 three possible ranges of loci for the object in a color-magnitude diagram (CMD), based on our assumptions about the amount of reddening, as discussed in Section 3.3.

We compared these loci in Figure 9 with single-star evolutionary tracks from the Modules for Experiments in Stellar Astrophysics (MESA) Isochrones and Stellar Tracks (MIST; Paxton et al. 2011; 2013; 2015; Choi et al. 2016) v1.1 with rotation at $v_{\mathrm{rot}}/v_{\mathrm{critical}} = 0.4$, solar-scaled abundances (assuming $Z = 0.0142$; Asplund et al. 2009), and subsolar metallicity $[\mathrm{Fe/H}] = -0.10$. The tracks have been interpolated to the WFPC2 VEGAMAG system by the MIST online in-

terface[10]. Among the tracks, we find that the candidate's locus, assuming the lowest reddening, is roughly consistent with, although somewhat blueward of, the terminus of a star with initial mass 48–$49\,M_\odot$. The net effect of rotation is to lead to a bigger He core mass, and thus more luminous progenitor, for the same initial mass. If the star was not a rapid rotator, then the implied initial mass (if single) would be even higher. We note that some evolutionary models for single stars with these initial masses at solar metallicity experience "failed" explosions, with the cores collapsing directly to black holes (e.g., Sukhbold et al. 2016).

Additionally, we compared in Figure 9 with the endpoints of binary-star models from BPASS v2.1 (Eldridge et al. 2017) at two different metallicities, solar and somewhat subsolar (note that for BPASS, $Z = 0.020$ is considered solar metallicity). What is shown in the figure is the combined light of both the primary and the secondary in each of the binary models. (Here we have assumed that the F555W and F814W bandpasses used for BPASS are generic enough to apply for WFPC2.) We have considered only systems for which the primary's surface H mass fraction $= 0$, surface He mass fraction ≤ 0.27, and the ratio of the mass of remaining He to the total ejecta mass ≤ 0.1 at the model endpoint. These criteria should be sufficient to approximate a He-stripped SN Ic progenitor (J. J. Eldridge, private communication). The systems allowed by the color and luminosity range for the progenitor, again assuming the lowest reddening, are to the lower-right corner of this color-luminosity range. At $Z = 0.020$ the lone system has a $60\,M_\odot$ primary, a mass ratio of the two components $q = 0.9$ (i.e., the system consists of two stars of nearly the same mass), and initial orbital period $\log P(\mathrm{day}) = 1.0$. The primary of this system ejects $M_{\mathrm{ej}} \approx 10\,M_\odot$ and leaves behind a remnant with $\sim 6\,M_\odot$. At $Z = 0.014$ there is one system with these same parameters, as well as systems with a $80\,M_\odot$ primary, $q = 0.7$, and a range of $\log P = 0.8$ to 2.0. These primaries eject $M_{\mathrm{ej}} \approx 6\,M_\odot$ and have remnants with ~ 7–$15\,M_\odot$. At $Z = 0.010$ the systems have primaries which, similarly, range from 60 to $80\,M_\odot$, with $q = 0.7$–0.8, and $\log P = 1$–2.8. Ejecta masses are in the range 5–$8\,M_\odot$, and remnant masses are ~ 8–$12\,M_\odot$. The remnants for all of these systems are most likely to be black holes.

It may seem counterintuitive that the model binary systems should possess a primary that is more massive than the single-star models, with both binary and single-

---

[10] http://waps.cfa.harvard.edu/MIST/.

star models having essentially the same observed luminosity in F814W at their endpoints. However, it should be remembered that what we are showing in Figure 9 is a CMD and not a Hertzsprung-Russell diagram (HRD). For all of the binary models considered here, the mass transfer is generally nonconservative: The more massive primaries in the models all lose substantial amounts ($\gtrsim 75\%$) of their initial mass, while the secondaries increase little in mass as the systems evolve. On a HRD the primaries end up being less luminous bolometrically, although far hotter ($T_{\rm eff} > 10^5$ K), than they were on the zero-age main sequence; the secondaries generally increase monotonically in luminosity, while changing little in effective temperature, ending up more luminous than the primaries. In fact, the model primaries in the binary systems end up less luminous than the endpoints of the single-star models. In the CMD shown in the figure, the secondaries all dominate the observed light of the systems at their endpoints; as an additional effect, the hot, stripped primaries contribute comparatively far less light at F814W.

It appears that the two highest-reddening scenarios, $A_V = 1.3$–1.9 mag for $R_V = 3.3$–6.8 and $A_V = 1.3$–1.7 mag at $R_V = 4.3$, imply that the object would be too blue and possibly too luminous for single stars or binary star systems. The lowest-reddening scenario also may be just on the verge of being too blue and luminous.

In addition, we cannot rule out that the progenitor candidate is actually a compact cluster. At the distance of NGC 3938, such a cluster could be unresolved. To that end, we considered stellar clusters in a galaxy similar to NGC 3938, those in NGC 628 (M74; also a nearly face-on Sc galaxy, but closer to us at 10.19 Mpc; Jang & Lee 2014), which Adamo et al. (2017) studied (see also Grasha et al. 2015). We considered the "default," or "reference" deterministic catalog, for which the cluster photometry is an averaged aperture correction method, and for which Milky Way extinction and Padova stellar evolutionary tracks for age-dating are adopted[11]. We selected from the catalog only those clusters that are symmetric, compact ones and include these for comparison in Figure 9. (Here we neglected differences in the F555W and F814W bandpasses between WFC3/UVIS and WFPC2.) We have dereddened the clusters, using the "best $E(B-V)$" in the catalog and assuming $R_V = 3.1$. Note that ~ 5 of these clusters are also roughly consistent with the possible loci for the progenitor. These particular clusters are all quite blue and young, with estimated ages $\lesssim 4$ Myr and masses
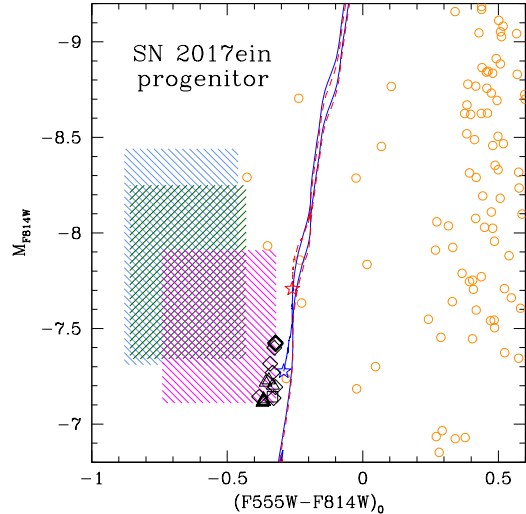
Figure 9. Color-magnitude diagram, in *HST* WFPC2 bands, showing three possible ranges in loci for the SN 2017ein progenitor candidate as hashed regions: (1) for $A_V = 1.3$–1.9 mag and $R_V = 3.3$–6.8, light blue; (2) for $A_V = 1.3$–1.7 mag fixed at $R_V = 4.3$, dark green; and, (3) for $A_V = 1.0$–1.2 mag fixed at $R_V = 3.1$, magenta. Also included in these ranges is the uncertainty in the distance to the host galaxy. Shown for comparison are single-star MIST evolutionary tracks (Paxton et al. 2011; 2013; 2015; Choi et al. 2016) for 48 $M_\odot$ (red dashed curve) and 49 $M_\odot$ (blue solid curve); the endpoint of each track is indicated with a star. Additionally, we show the endpoints of model binary systems from BPASS v2.1 (Eldridge et al. 2017) at three possible metallicities, $Z = 0.020$ (open square), $Z = 0.014$ (open triangles), and $Z = 0.010$ (open diamonds). The colors and magnitudes of stellar clusters in NGC 628 (M74) identified by Adamo et al. (2017) are represented by orange open circles. See text for details.

$\lesssim 2000$ $M_\odot$. Based on the MIST tracks, the turnoff masses for such young clusters are $\gtrsim 65$ $M_\odot$.

4.4. *Constraints from the Stellar Environment*

We can also potentially constrain the initial mass of the SN 2017ein progenitor by estimating the age of the stellar population, or populations, in its immediate environment. Here we consider a radius from the SN position for the environment of ~ 100 pc, a typical size for an OB association, within which stars should generally be coeval with the progenitor. We had already extracted the photometry from the archival *HST* WFPC2 images for the environment, as well as for the progenitor (Section 4.1). All of these objects appear to be point-like, based on their Dolphot photometric properties, discussed above. We show in Figure 10 a CMD displaying the objects in the environment, corrected by two different assumptions of the total visual extinction, $A_V = 1$ and 2 mag, and adjusted by the as-

sumed distance (the uncertainty in the distance is included in the uncertainties in absolute magnitude). A Cardelli, Clayton, & Mathis (1989) reddening law was assumed here with $R_V = 3.1$. We note, of course, that this is a simplification, since, over this size scale the extinction could be variable. The photometry for the progenitor candidate is included in the figure, but corrected for reddening by the same amounts as the overall environment, not as we have done in Section 4.3.

One can see a number of stellar objects in the SN 2017ein environment. One interesting inference to point out is that, although the progenitor candidate may be among the bluest objects in the environment, it is not necessarily the most luminous. We have compared the photometry for these objects with the PARSEC-COLIBRI model isochrones from Marigo et al. (2017) and MIST isochrones from Choi et al. (2016), both at a subsolar metallicity $Z = 0.01$. Note that these models are all based on single-star evolutionary tracks. We can approximately fit these populations, using both sets of models, with a mix of three different ages (4, 7, and 13 Myr), if the extinction is $A_V \approx 1$ mag. The objects are poorly fit if A_V were closer to 2 mag, particularly for the objects with $(F555W-F814W)_0 < 0$ mag, which are likely massive main-sequence stars. We therefore consider this assumed extinction to be an upper limit on the actual extinction. Assuming the lower extinction, the youngest objects are generally quite blue. Three evolved cool supergiants appear consistent with the 13 Myr isochrone, with one or two additional objects consistent with the blue loop of the PARSEC-COLIBRI track at that age.

The corresponding turnoff masses for the PARSEC-COLIBRI isochrones are ~ 57, 28, and 16 $M_\odot$. These masses are quite similar for the MIST isochrones, at ~ 60, 26, and 15 $M_\odot$. That a SN has occurred recently in this environment would imply that it is a member of the younger, more massive population. The inferred initial masses are consistent with those of the high-mass BPASS binary models that appear to agree with the locus of the progenitor candidate in the CMD. However, if the assumption of coevality breaks down (for example, dispersal through random motions), then it is possible that the SN progenitor was a member of one of the older, less massive populations, consistent with the expectation of a more moderate-mass binary progenitor. Furthermore, Maund (2017) showed that, within 100 pc in the environments of SNe II-P, a mixture of populations at different ages could be colocated, one of those populations being related to a given SN II-P progenitor. A similar situation might be in effect for the SN 2017ein environment.
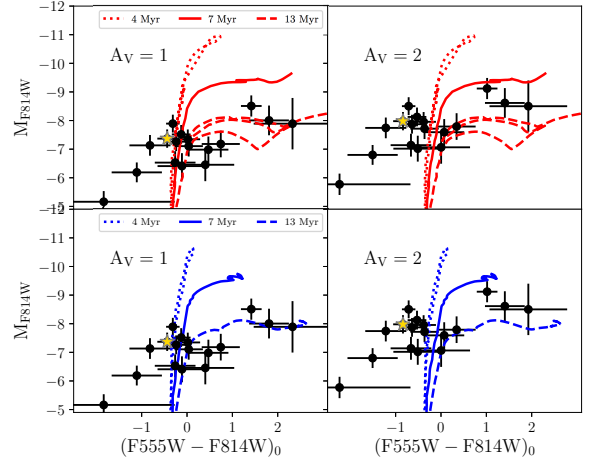

Figure 10. Color-magnitude diagrams of the stellar environment (points) within ~ 100 pc of SN 2017ein, based on the *HST* photometry, corrected by different assumptions for total visual extinction and analyzed with different model isochrones. The uncertainty in the distance to NGC 3938 is included in the uncertainties in absolute magnitude. The left panels assume $A_V = 1$ mag toward the environment; the right panels assume $A_V = 2$ mag. The top panels show PARSEC-COLIBRI isochrones (Marigo et al. 2017; red curves), and the bottom panels show MIST isochrones (Choi et al. 2016; blue curves), at $Z = 0.01$ with ages 4, 7, and 13 Myr. The progenitor candidate is indicated by the yellow (light) star and has been reddening-corrected by the same amount as the overall environment.

5. DISCUSSION

We have found that SN 2017ein in NGC 3938 appears to be similar, both photometrically and spectroscopically, to SN 2007gr during approximately its first month since explosion. We have also compared SN 2017ein to SN 2004aw, to which it bears more similarity spectroscopically than photometrically. Uncertainty exists in the value of the extinction to SN 2017ein. We have attempted to estimate the extinction from the strength of the Na I D absorption in the spectra, as well as via comparisons of the object's colors with those of SN 2007gr and a $B - V$ color template for SNe Ic assembled by Stritzinger et al. (2018). We were only able to establish a range in A_V, together with a possible range in R_V. Given the uncertainties in the overall reddening and in the distance to the host galaxy, we found that, bolometrically, SN 2017ein is somewhat more luminous than SN 2007gr and could be as luminous as SN 2004aw. We estimated $M(^{56}\mathrm{Ni})$, M_{ej}, and E_K, which are reasonably consistent with the estimates for previous SNe Ic.

We have also identified a progenitor candidate in archival *HST* WFPC2 imaging. This potentially constitutes the first time that a progenitor candidate has

ever been identified for a SN Ic. Based on the assumed ranges in both distance and extinction to the SN, we infer that the progenitor candidate is quite luminous and blue, possibly more so than we would have expected, based on models of their progenitors. Comparison with both single-star evolutionary tracks and the endpoints of binary-star models would imply that the progenitor is very massive, with initial mass $\sim 49\ M_\odot$, if single, and possibly as high as 80 $M_\odot$, if the primary is in a binary system. This is far more massive than what we infer to be the initial masses of the progenitors of the more common SNe II-P and also of SNe IIb and Ib (although the true nature of the sole known SN Ib progenitor, of iPTF13bvn, is still to be established). Such a high mass would be consistent with what Maund & Ramirez-Ruiz (2016) concluded for the progenitor of SN 2007gr, that it had to be quite massive, $M_{\mathrm{ZAMS}} \approx 30\ M_\odot$, based on an analysis of that object's stellar environment. However, we note that Mazzali et al. (2010) tallied up $\sim 1\ M_\odot$ of ejecta for SN 2007gr from late-time spectra and concluded that the progenitor was a star of relatively low initial mass ($\sim 15\ M_\odot$).

We also considered the possibility that the observed object is a compact cluster, rather than a star or stellar system. We compared the candidate to observations of compact clusters in a galaxy similar in characteristics to the SN host. We found that the progenitor candidate is roughly consistent with among the bluest and youngest clusters, with very high turnoff masses, which would, again, imply a high-mass progenitor for SN 2017ein. If it were a very young, blue cluster, we might expect interstellar Hα emission at the site. We indeed detect such emission, particularly in the early-time MMT spectrum, and we estimate from the observed flux in the Hα line, the Hα luminosity to be $L_{\mathrm{H}\alpha} \approx 6.7 \times 10^{49}$ to 2.5×10^{50} erg s^{-1}, given the range of assumed reddening and distance. Assuming the number of Lyman continuum photons $N_{\mathrm{LyC}} = 7.25 \times 10^{11}\ L_{\mathrm{H}\alpha}$, and adopting the stellar parameters from Martins et al. (2005), this is the equivalent of 1–4 O3 I stars, or 4–15 O5 V stars. The source of the ionization, then, either could be from a hot, luminous binary system or a compact cluster of a few massive stars. The H II region is not detected in a ground-based Hα image from 2002 of the host galaxy[12] obtained by the SINGS project (Kennicutt et al. 2003). The FWHM of the object is $\sim 0\rlap{.}''15$ at the WFPC2 scale, which, at the distance of NGC 3938, is ~ 12–16 pc. For the sample of clusters in M74, those considered compact have effective radii $\lesssim 3$ pc (Ryon et al. 2017). So, it is plausible that

a massive progenitor system for SN 2017ein could be in the environment of a putative compact cluster and not be an actual member. (Again, we note the 0.22 pixel, or 22 mas, offset between the SN and progenitor candidate positions in the *HST* imaging, which although within the measurement uncertainties, would represent an additional spatial offset of ~ 1–2 pc.) Such a progenitor system in a presumably actively star-forming environment along a spiral arm could still be massive, just not necessarily from the same population and not necessarily of high mass. We are not in a position, based on the available data, to constrain such a system further.

An important test will be to return to the site years from now when the SN has faded, ideally either with *HST* or the *James Webb Space Telescope*, and determine whether the progenitor candidate still persists. We note, however, that if the BPASS binary models are correct, a luminous secondary could still be evident at the SN location (at the assumed distance range to the SN, a companion will not have perceptively drifted from its current position, as a result of a SN kick; the energy imparted on such a companion would also likely not be enough to modify its luminosity significantly), and the overall brightness of the object may have dimmed some, but not completely. From the BPASS models, such a surviving companion would have apparent F814W ≈ 25.9–24.6 and F555W$-$F814W ≈ 0.2–0.4 mag observed with WFC3/UVIS.

The inferred color and luminosity of the object may inevitably have been too blue and luminous to be physically realistic. The largest systematic uncertainty in the analysis is almost certainly in our estimate of the extinction to SN 2017ein. The upper limit on the presence of the DIB $\lambda 5780$ feature in the MMT spectrum, for instance, seems to indicate that A_V could be $\lesssim 1.1$ mag. It is therefore important to better establish both the extinction and the distance to this SN. We have made the best effort given the data we had available. It is possible that we have misestimated the reddening by using the intrinsic color curves for SN 2007gr and the reddening-free SN Ic color template from Stritzinger et al. (2018). Also, the host galaxy is likely beyond a practical distance for a tip-of-the-red-giant-branch (TRGB) measurement of its distance; however, the discovery and use of Cepheid variables via space-based observations is still possible.

Finally, we note in passing that the observations of SN 2017ein do not match well with the recent radiative-transfer models for SESNe by Dessart et al. (2016). Although their relation between $M_R(\mathrm{max})$ and $M(^{56}\mathrm{Ni})$ predicts ~ 0.06–0.10 $M_\odot$, consistent with the results of our bolometric light-curve fitting and R-band light-

---

[12] Available via NED.

curve analysis, none of their model bolometric light curves provides a good match to that for SN 2017ein. Similarly, their model relation between the velocity at maximum light from the O I λ7774 line and the SN expansion rate does not hold for this SN; at R-band maximum we measure a velocity in this line of $\sim 9800\,\mathrm{km\,s^{-1}}$, which is well off the trend shown by Dessart et al. (2016; their Figure 16).

Facilities: HST (WFPC2, WFC3), KAIT, Nickel, Shane (Kast Spectrograph), MMT (Blue Channel spectrograph)

Software: AstroDrizzle(Hack et al. 2012; http://drizzlepac.stsci.ed Dolphot (Dolphin 2016), DAOPHOT (Stetson 1987), IRAF(Tody 1986; 1993), PyRAF(http://www.stsci.edu/institute/sof extinction(Barbary 2016; https://github.com/kbarbary/extinction), galflat(http://idlastro.gsfc.nasa.gov/ftp/pro/astro/gal_flat.pro), ishivvers/TheKastShiv(https://github.com/ishivvers/TheKastShiv pysynphot(Lim et al. 2015; https://github.com/spacetelescope/pysyn

REFERENCES

Abbott, B. P., Abbott, R., Abbott, T. D., et al. 2017, ApJL, 848, L12

Adamo, A., Ryon, J. E., Messa, M., et al. 2017, ApJ, 841, 131

Arbour, R. 2017, Transient Name Server Discovery Report, 588

Arnett, W. D. 1982, ApJ, 253, 785

Arnett, W. D., Fryer, C., & Matheson, T. 2017, ApJ, 846, 33

Asplund, M., Grevesse, N., Sauval, A. J., & Scott, P. 2009, ARA&A, 47, 481

18

Barbary, K. 2016, extinction, v0.3.0, Zenodo,
doi: 10.5281/zenodo.804967.
https://github.com/kbarbary/extinction

Benvenuto, O. G., Bersten, M. C., & Nomoto, K. 2013,
ApJ, 762, 74

Bersten, M. C., Folatelli, G., García, F., et al. 2018,
Nature, 554, 497

Bertola, F. 1963, Mem. Soc. Astron. Italiana, 34, 33

Bertola, F., Mammano, A., & Perinotto, M. 1965,
Contributi dell'Osservatorio Astrofisica dell'Universita di
Padova in Asiago, 174, 3

Bianco, F. B., Modjaz, M., Hicken, M., et al. 2014, ApJS,
213, 19

Bottinelli, L., Gouguenheim, L., Paturel, G., & de
Vaucouleurs, G. 1984, A&AS, 56, 381

Bottinelli, L., Gouguenheim, L., Paturel, G., & Teerikorpi,
P. 1986, A&A, 156, 157

Cano, Z. 2013, MNRAS, 434, 1098

Cao, Y., Kasliwal, M. M., Arcavi, I., et al. 2013, ApJL, 775,
L7

Cardelli, J. A., Clayton, G. C., & Mathis, J. S. 1989, ApJ,
345, 245

Chatzopoulos, E., Wheeler, J. C., & Vinko, J. 2012, ApJ,
746, 121

Chen, J., Wang, X., Ganeshalingam, M., et al. 2014, ApJ,
790, 120

Choi, J., Dotter, A., Conroy, C., et al. 2016, ApJ, 823, 102

Dessart, L., Hillier, D. J., Li, C., & Woosley, S. 2012,
MNRAS, 424, 2139

Dessart, L., Hillier, D. J., Woosley, S., et al. 2016, MNRAS,
458, 1618

Dolphin, A. E. 2000a, PASP, 112, 1383

Dolphin, A. 2016, Astrophysics Source Code Library,
ascl:1608.013

Drout, M. R., Soderberg, A. M., Gal-Yam, A., et al. 2011,
ApJ, 741, 97

Eldridge, J. J., & Maund, J. R. 2016, MNRAS, 461, L117

Eldridge, J. J., Fraser, M., Smartt, S. J., Maund, J. R., &
Crockett, R. M. 2013, MNRAS, 436, 774

Eldridge, J. J., Stanway, E. R., Xiao, L., et al. 2017, PASA,
34, e058

Elias-Rosa, N., Pastorello, A., Maund, J. R., et al. 2013,
MNRAS, 436, L109

Filippenko, A. V. 1982, PASP, 94, 715

Filippenko, A. V. 1997, ARAA, 35, 309

Filippenko, A. V., Li, W. D., Treffers, R. R., & Modjaz, M.
2001, IAU Colloq. 183: Small-Telescope Astronomy on
Global Scales, 246, 121

Fitzpatrick, E. L. 1999, PASP, 111, 63

Folatelli, G., Bersten, M. C., Kuncarayakti, H., et al. 2015,
ApJ, 811, 147

Folatelli, G., Van Dyk, S. D., Kuncarayakti, H., et al. 2016,
ApJL, 825, L22

Gal-Yam, A., Fox, D. B., Kulkarni, S. R., et al. 2005, ApJL,
630, L29

Gal-Yam, A., Bufano, F., Barlow, T. A., et al. 2008, ApJL,
685, L117

Ganeshalingam, M., Li, W., Filippenko, A. V., et al. 2010,
ApJS, 190, 418

Georgy, C., Meynet, G., Walder, R., Folini, D., & Maeder,
A. 2009, A&A, 502, 611

Grasha, K., Calzetti, D., Adamo, A., et al. 2015, ApJ, 815,
93

Graur, O., Bianco, F. B., Huang, S., et al. 2017, ApJ, 837,
120

Hachinger, S., Mazzali, P. A., Taubenberger, S., et al. 2012,
Death of Massive Stars: Supernovae and Gamma-Ray
Bursts, 279, 122

Hack, W. J., Dencheva, N., Fruchter, A. S., et al. 2012,
American Astronomical Society Meeting Abstracts #220,
220, 135.15

Hjorth, J., & Bloom, J. S. 2012, Chapter 9 in "Gamma-Ray
Bursts", Cambridge Astrophysics Series 51,
eds. C. Kouveliotou, R. A. M. J. Wijers and S. Woosley,
Cambridge University Press (Cambridge), p. 169-190

Hunter, D. J., Valenti, S., Kotak, R., et al. 2009, A&A, 508,
371

Im, M., Choi, C., Lee, S.-Y., et al. 2017, The Astronomer's
Telegram, No. 10481

Jang, I. S., & Lee, M. G. 2014, ApJ, 792, 52

Jarrett, T. H., Chester, T., Cutri, R., Schneider, S. E., &
Huchra, J. P. 2003, AJ, 125, 525

Johnson, S. A., Kochanek, C. S., & Adams, S. M. 2017,
MNRAS, 472, 3115

Kennicutt, R. C., Jr., Armus, L., Bendo, G., et al. 2003,
PASP, 115, 928

Kim, H.-J., Yoon, S.-C., & Koo, B.-C. 2015, ApJ, 809, 131

Lim, P. L., Diaz, R. I., & Laidler, V. 2015, PySynphot
Users Guide (Baltimore, MD: STScI).
https://pysynphot.readthedocs.io/en/latest/

Liu, Y.-Q., Modjaz, M., Bianco, F. B., & Graur, O. 2016,
ApJ, 827, 90

Lyman, J. D., Bersier, D., & James, P. A. 2014, MNRAS,
437, 3848

Lyman, J. D., Bersier, D., James, P. A., et al. 2016,
MNRAS, 457, 328

Marigo, P., Girardi, L., Bressan, A., et al. 2017, ApJ, 835,
77

Marino, R. A., Rosales-Ortega, F. F., Sánchez, S. F., et al. 2013, A&A, 559, A114

Martins, F., Schaerer, D., & Hillier, D. J. 2005, A&A, 436, 1049

Massey, P., & Johnson, O. 1998, ApJ, 505, 793

Maund, J. R. 2017, MNRAS, 469, 2202

Maund, J. R., Smartt, S. J., & Schweizer, F. 2005, ApJL, 630, L33

Maund, J. R., Fraser, M., Ergon, M., et al. 2011, ApJL, 739, L37

Maund, J. R., & Ramirez-Ruiz, E. 2016, MNRAS, 456, 3175

Mazzali, P. A., Maurer, I., Valenti, S., Kotak, R., & Hunter, D. 2010, MNRAS, 408, 87

Mazzali, P. A., Sauer, D. N., Pian, E., et al. 2017, MNRAS, 469, 2498

Milisavljevic, D., Margutti, R., Crabtree, K. N., et al. 2014, ApJL, 782, L5

Miller, J. S., & Stone, R. P. S. 1993, Lick Obs. Tech. Rep. 66 (Santa Cruz: Lick Obs.)

Nomoto, K., Filippenko, A. V., & Shigeyama, T. 1990, A&A, 240, L1

Nomoto, K., Yamaoka, H., Pols, O. R., et al. 1994, Nature, 371, 227

Paxton, B., Bildsten, L., Dotter, A., et al. 2011, ApJS, 192, 3

Paxton, B., Cantiello, M., Arras, P., et al. 2013, ApJS, 208, 4

Paxton, B., Marchant, P., Schwab, J., et al. 2015, ApJS, 220, 15

Pettini, M., & Pagel, B. E. J. 2004, MNRAS, 348, L59

Phillips, M. M., Simon, J. D., Morrell, N., et al. 2013, ApJ, 779, 38

Pilyugin, L. S., Grebel, E. K., & Kniazev, A. Y. 2014, AJ, 147, 131

Podsiadlowski, P., Hsu, J. J. L., Joss, P. C., & Ross, R. R. 1993, Nature, 364, 509

Pols, O. R., & Dewi, J. D. M. 2002, PASA, 19, 233

Poznanski, D., Butler, N., Filippenko, A. V., et al. 2009, ApJ, 694, 1067

Prentice, S. J., Mazzali, P. A., Pian, E., et al. 2016, MNRAS, 458, 2973

Rodríguez, Ó., Clocchiatti, A., & Hamuy, M. 2014, AJ, 148, 107

Ryon, J. E., Gallagher, J. S., Smith, L. J., et al. 2017, ApJ, 841, 92

Schlafly, E. F., & Finkbeiner, D. P. 2011, ApJ, 737, 103

Shara, M. M., Bibby, J. L., Zurek, D., et al. 2013, AJ, 146, 162

Shivvers, I., Zheng, W., Van Dyk, S. D., et al. 2017, MNRAS, 471, 4381

Silverman, J. M., Foley, R. J., Filippenko, A. V., et al. 2012, MNRAS, 425, 1789

Smartt, S. J., Eldridge, J. J., Crockett, R. M., & Maund, J. R. 2009, MNRAS, 395, 1409

Smartt, S. J. 2015, PASA, 32, e016

Smith, N. 2002, MNRAS, 331, 7

Smith, N., Li, W., Filippenko, A. V., & Chornock, R. 2011, MNRAS, 412, 1522

Stancliffe, R. J., & Eldridge, J. J. 2009, MNRAS, 396, 1699

Stetson, P. B. 1987, PASP, 99, 191

Stritzinger, M. D., Taddia, F., Burns, C. R., et al. 2018, A&A, 609, A135

Sukhbold, T., Ertl, T., Woosley, S. E., Brown, J. M., & Janka, H.-T. 2016, ApJ, 821, 38

Taddia, F., Sollerman, J., Leloudas, G., et al. 2015, A&A, 574, A60

Taubenberger, S., Pastorello, A., Mazzali, P. A., et al. 2006, MNRAS, 371, 1459

Tody, D. 1986, Proc. SPIE, 627, 733

Tody, D. 1993, Astronomical Data Analysis Software and Systems II, 52, 173

Tonry, J. L., Stubbs, C. W., Lykke, K. R., et al. 2012, ApJ, 750, 99

Tsvetkov, D. Y., Volnova, A. A., Shulga, A. P., et al. 2006, A&A, 460, 769

Tully, R. B. 1988, Nearby Galaxies Catalog (Cambridge: Cambridge University Press)

Valenti, S., Elias-Rosa, N., Taubenberger, S., et al. 2008, ApJL, 673, L155

Vacca, W. D., & Leibundgut, B. 1997, NATO Advanced Science Institutes (ASI) Series C, 486, 65

Van Dyk, S. D., Li, W., Cenko, S. B., et al. 2011, ApJL, 741, L28

Van Dyk, S. D., Zheng, W., Fox, O. D., et al. 2014, AJ, 147, 37

Van Dyk, S. D., Filippenko, A. V., Fox, O. D., et al. 2017, The Astronomer's Telegram, No. 10485

Wellstein, S., & Langer, N. 1999, A&A, 350, 148

Wheeler, J. C., Johnson, V., & Clocchiatti, A. 2015, MNRAS, 450, 1295

Williams, P. M. 2008, Revista Mexicana de Astronomia y Astrofisica Conference Series, 33, 71

Ziang, D., Song, H., Wang, X., et al. 2017, The Astronomer's Telegram, No. 10434

Yaron, O., & Gal-Yam, A. 2012, PASP, 124, 668

Yoon, S.-C., Woosley, S. E., & Langer, N. 2010, ApJ, 725, 940

Yoon, S.-C., Gräfener, G., Vink, J. S., Kozyreva, A., & Izzard, R. G. 2012, A&A, 544, L11

Zapartas, E., de Mink, S. E., Van Dyk, S. D., et al. 2017,
ApJ, 842, 125

All Authors and Affiliations

Schuyler D. Van Dyk,[1] WeiKang Zheng,[2] Thomas G. Brink,[2] Alexei V. Filippenko,[3,4] Dan Milisavljevic,[5] Jennifer E. Andrews,[6] Nathan Smith,[6] Michele Cignoni,[7,8] Ori D. Fox,[9] Patrick L. Kelly,[2,10] Angela Adamo,[11] Sameen Yunus,[2] Keto Zhang,[2] and Sahana Kumar[2,12]

[1]*Caltech/IPAC, Mailcode 100-22, Pasadena, CA 91125, USA 0000-0001-9038-9950*

[2]*Department of Astronomy, University of California, Berkeley, CA 94720-3411, USA*

[3]*Department of Astronomy, University of California, Berkeley, CA 94720-3411, USA 0000-0003-3460-0103*

[4]*Miller Senior Fellow, Miller Institute for Basic Research in Science, University of California, Berkeley, CA 94720, USA*

[5]*Department of Physics and Astronomy, Purdue University, 525 Northwestern Avenue, West Lafayette, IN 47907, USA*

[6]*Steward Observatory, University of Arizona, 933 N. Cherry Avenue, Tucson, AZ 85721, USA*

[7]*Dipartimento di Fisica 'Enrico Fermi', Universitá di Pisa, largo Pontecorvo 3, I-56127 Pisa, Italy 0000-0001-6291-6813*

[8]*INFN, Largo B. Pontecorvo 3, I-56127 Pisa, Italy*

[9]*Space Telescope Science Institute, 3700 San Martin Drive, Baltimore, MD 21218, USA 0000-0002-4924-444X*

[10]*College of Science & Engineering, Minnesota Institute for Astrophysics, University of Minnesota, 115 Union St. SE, Minneapolis, MN 55455 USA 0000-0003-3142-997X*

[11]*Department of Astronomy, Oskar Klein Centre, Stockholm University, AlbaNova University Centre, SE-106 91 Stockholm, Sweden 0000-0002-8192-8091*

[12]*Department of Physics, Florida State University, 77 Chieftain Way, Tallahassee, Florida 32306, USA*